

# sA Unified Design of ACO and Skewness based Brain Tumor Segmentation and Classification from MRI Scans

Umaira Nazar Hussain<sup>1</sup>, Muhammad Attique Khan<sup>2</sup>, Ikram Ullah Lali<sup>3</sup>, Kashif Javed<sup>4</sup>, Imran Ashraf<sup>5</sup>, Junaid Tariq<sup>6</sup>, Hashim Ali<sup>7</sup>, Ahmad Din<sup>8</sup>

<sup>1</sup> Department of CS & IT, University of Sargodha, Pakistan

<sup>2,6</sup> Department of Computer Science, HITEC University, Museum Road, Taxila, Pakistan

<sup>3</sup> Department of Information Technology, University of Education, Jauharabad Campus, Khushab, Pakistan

<sup>4</sup> Department of Robotics, SMME NUST Islamabad, Pakistan

<sup>5,7</sup> Department of Computer Engineering, HITEC University, Museum Road, Taxila, Pakistan

<sup>8</sup> Department of CS, COMSATS University Islamabad, Abbottabad Campus

Corresponding Author\*: attique@ciitwah.edu.pk

**Abstract:** Brain tumor is among the major reasons for deaths among cancerous diseases around the world. Medical imaging technologies used to detect brain tumor is very popular these days. However, before time detection is open-ended research and needs to be handled more accurately. Multimodality medical image fusion has emerged with promising results in cancer detection. In this paper, a hybrid technique for extracting tumors using MRI images is presented. This technique consists of five steps, such as de-noising of an image, the extraction of the tumor, feature selection, feature fusion, and classification. Curvelet transformation is implemented in the first step for image de-noising. Then in the second step, Ant Colony Optimization (ACO) is utilized along with the Thresholding method for the extraction of tumors based on MRI scans of the brain. Three distinct kinds of features are extracted depending on texture and shape in the third step. After that, the top 70% features are selected based on the priority approach, and fusion is performed using a concatenation based approach. In the last step, fused features are fed to different classifiers such as SVM. The proposed technique is tested on two datasets named BRATS2013 and private dataset. This new system performed well in comparison to different present systems.

**Keywords:** Brain Tumor; Tumor segmentation; Feature extraction; Features Reduction; Classification

## 1. INTRODUCTION

A brain tumor is a collection of unusual or uncommon cells present inside the brain area. The rigid outer covering of the brain, which plays a role of protector for it in case of an injury, is its skull. Any abnormal growth of cells inside it will cause a severe problem (Fernandes et al., 2019; Khan et al., 2019). The brain tumor is of two types- malignant, which is more dangerous and difficult to cure, while the second type is benign, which is curable if detected at the initial stage (M. I. Sharif et al., 2020). Moreover, the brain tumor has two categories, known as primary and metastatic. The primary brain tumor starts within the brain due to the abnormal growth of brain cells, but in contrast, metastatic starts when cancer cells from other parts of the body are fragmented and travel towards the brain. Due to this reason, metastatic brain tumors always lie in the category of a malignant but primary brain tumor cannot be malignant all time, it may lie in benign too (Liu et al., 2014). Treatment of brain tumors varies according to its categories. In the United States, currently, around 700,000 people are diagnosed with primary brain cancer, and more than 790,000 will be identified in 2018 (Buerki et al., 2018). The brain tumor has a great psychological, physical, plus cognitive influence on the quality of a patient's life as well as it totally alters everything for patients and their relatives.

Brain tumors are classified according to tumor location, tissues involved, and the type of tumor that is benign or malignant. The selection of treatment therapy for a brain tumor depends upon the size, location, and growth rate (Anitha et al., 2018). The World Health Organization (WHO) presented the scheme of grading the tumors in the brain. According to this scheme, tumors are categorized in four grades under a microscope, and these grades are given names as I, II, III, and IV grade, respectively. Furthermore, a benign tumor is known as a low-grade brain tumor because it consists of both I grade as well as II grade tumors. While on the other side, a malignant tumor is known as a high-grade brain tumor because it has tumors of III grade and IV grade. The rate to detect low-grade brain tumors at the starting stage or initial stage is very low and hence it gets converted to high-grade brain tumors (Roberts et al., 2018). The brain image of malignant tumor, healthy brain, and benign tumor are shown in Figure 1. Magnetic resonance image (MRI), as well as Computed Tomography (CT), are two frequently used modalities of imaging which play a vibrant role for detecting a tumor in the brain (Drozdal et al., 2018). MRI scan of brain and CT both help doctors to identify and find the exact position plus magnitude of a tumor inside a brain. MRI is a modality with improved contrast of soft tissues as well as its non-invasive behavior, which gives details about tumor

location, shape, and size in the absence of high ionization radiations (Mohsen et al., 2018).

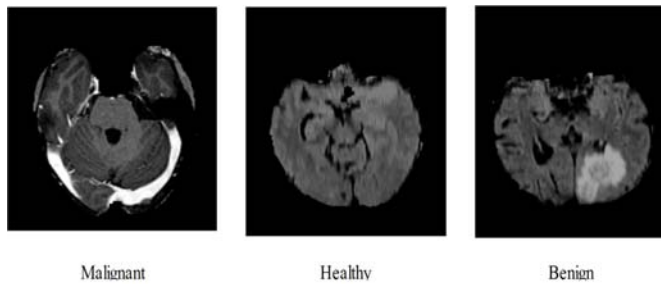


Fig. 1. Sample brain tumor MRI images.

MRI images have some benefits as compared to other modality images because these images help doctors to detect the tumor at an initial stage by giving a clear image with more details (Kalavathi and Prasath, 2016). The MRI images are classified into four modalities, which are known as T1 modality, T1c modality, T2 modality, and T2f modality, respectively. Further, these modalities play a prominent part in detecting the affected area by tumor from the brain image. The sample scans are shown in Figure 2.

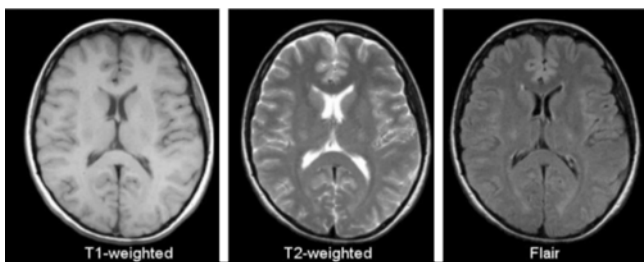


Fig. 2. Sample scans of brain modalities (Zhang et al., 2015).

Manual detection and segmentation of brain tumors do not provide accurate results, and it is time taking and slow process. The main limitation of the manual method is its irreducibility, which increases the demand for computer-based segmentation and classification. Moreover, tumor shape, tumor diameter, texture, size, location, and irregularity are common problems in existing systems. To overcome these problems, in this research, an amalgamation approach is utilized, which includes series of primary steps- Curvelet transform based tumor visibility enhancement, ACO and thresholding based tumor segmentation, texture and shape feature extraction, priority features selection and finally classification.

### 1.1 Major contributions

- Curvelet transform is employed to enhance the visibility of the original tumor from a distinct scale and angle.
- The tumor segmentation is performed through ACO along with the thresholding approach.
- Multi-type features are extracted like shape and texture. Then a new approach is applied named PCA reduced Skewness (PCArS) approach for irrelevant features reduction.
- A comparison is conducted with several classification methods and existing techniques for the validity

of this approach.

### 1.2 Problem Statement

In this work, our major focus is on the correct segmentation of brain tumors and later accurate classification into relevant categories. For this process, several challenges exist, such as low contrast tumor, tumor diameter, tumor size, irrelevant features, and few more. Whereas in this work, our focus is tumor enhancement and irrelevant features reduction for best segmentation and classification accuracy.

## 2. RELATED WORK

Automatic identification and classification of harmful human diseases such as brain tumor, stomach infections, skin cancer (Rehman et al., 2020) and lungs cancer are very common infections in medical imaging (Afza et al., 2019; Khan et al., 2019; Safdar et al., 2019). There exist several segmentation and classification methods based on machine learning (ML) and computer vision (CV) which are utilized for the diagnosis of these infections (Akram et al., 2018; Khan et al., 2018; Amna Liaquat et al., 2018; Nasir et al., 2018; M. Sharif et al., 2018).

The brain tumor is a critical and most dangerous type of cancer in medical imaging, and recently various computerized methods are introduced for its diagnosis. Generally, existing processes include many steps such as pre-processing for noise removal, segmentation of tumor area, useful features extraction, reduction of redundant features, and classification (Rashid et al., 2018). Ariyo et al. (Ariyo et al., 2017) introduced a technique named as SFCMKA (Spatial Fuzzy C-Means plus K-means Algorithm) for the separation of abnormal brain tissues from the healthy brain tissues. In this technique, the noise is mitigated due to the merging of spatial function to the FCM algorithm and maximum probability for pixels with singular membership is attained by using the K-means algorithm. Sharif et al. (Rashid et al., 2018) described improved binomial thresholding and multi-features selection approach for brain tumor segmentation. Gaussian filter is used for pre-processing and an improved thresholding technique with some morphological operations is utilized for tumor segmentation.

After that, a serial based method is implemented for the fusion of extracted geometric and Harlick features. Lastly, the selection of best features is performed from the fused vector using GA and classification is performed using LSVM on the basis of these best features. Damodharan et al. (Damodharan and Raghavan, 2015) introduced a brain tumor detection approach that depends on the integration of Tissue Segmentation and Neural Network. The performance of the implemented approach is measured by comparing its results with other classification approaches such as NN, KNN, and Bayesian classification with respect to the accuracy, specificity, and sensitivity. Pereira et al. (Pereira et al., 2016) implemented an approach based on Convolution Neural Networks (CNN) using MRI images for the accurate extraction of the tumor. Rajuet al. (Bahadure et al., 2018) implemented a classification method based on Bayesian fuzzy clustering to extract plus classify the tumor area from

the brain MRI scans. The presented method performance is good in terms of accuracy as compared to a few already implemented approaches. Sharma et al. (Sharma et al., 2018) introduced a hybrid approach extraction of tumor regions accurately as well as the classification of brain tumors. Three primary steps are involved in this presented approach- (a) Pre-processing which included thresholding, morphological operations and watershed segmentation (b) Segmented MRI scans are used for extraction of GLCM features, and (c) classification of tumor through KMNN classifier.

### 3. PROPOSED METHOD

There are five steps of the proposed system, including pre-processing of an input image, segmentation of tumor using ACO and thresholding, extraction of few useful features, best features selection based on high priority, and fusion of features. Later on, these features are given for the classification process to a classifier named Support Vector Machine (SVM). The demonstration of the flow of the proposed approach is presented in Fig. 3.

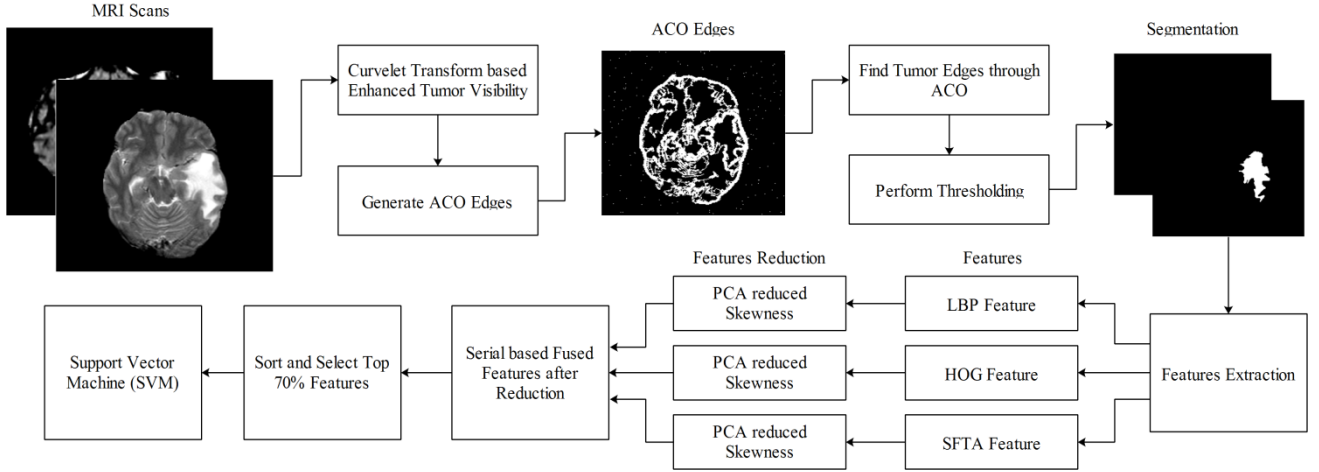


Fig. 3. Proposed brain tumor extraction and classification approach using MRI scans.

#### 3.1. Image Enhancement Using Curvelet Transform

Curvelet transform is implemented for mitigation of the unwanted noise from an input image of the brain by enhancing the tumor region. This enhancement technique is good in terms of implementation simplicity, disorder stability, and less processing time. Furthermore, maximum recovery of edges plus dim linear, as well as curve features, are attained in Curvelet transform. The use of ridgelet transforms Curvelet transform (Routray et al., 2018; Starck et al., 2002) efficient as compared to wavelet transform in terms of the best performance for image de-noising. The ridgelet transform is converted to a Radon transform. Anisotropy scaling relationship is performed to implement support interval or to scale in ridgelet transform. The curve or edge is decomposed into blocks and sub-blocks by applying a multi-scaling ridgelet. Further, these sub-blocks are roughly considered as straight lines for the implementation of ridgelet analysis. The decomposition stages of Curvelet transform are mathematically described as follows in equation (1).

$$g \mapsto (F_0 g, \Delta_1 g, \Delta_2 g, \dots) \quad (1)$$

Where,  $F_0$  denotes sub-bands filters,  $\Delta$  denotes information about sub-band  $2^{-2b}$  and  $g$  is an object like a tumor. The smooth windows are  $V_Q(k_1, k_2)$  and dyadic squares are used to localize these smoothing windows. The  $k_1$  and  $k_2$  are initialized based on the image size. The mathematical relation is explained below in equation (2).

$$Q = \left[ \frac{k_1}{2^b}, \frac{(k_1+1)}{2^b} \right] \times \left[ \frac{k_2}{2^b}, \frac{(k_2+1)}{2^b} \right] \quad (2)$$

After that, renormalization is performed on the resultant square to unit scale. The quantitative relation of this step is represented mathematically as follows.

$$h_Q = F^{-1}_Q(V_Q \Delta_b g), Q \in Q_b$$

Where,  $(F_Q g)(x_1, x_2) = 2^b g(2^b x_1 - K_1, 2^b x_2 - K_2)$  and demonstrates the renormalization operator. Here, two dyadic sub-bands  $[2^{2b}, 2^{2b+1}]$  and  $[2^{2b+1}, 2^{2b+2}]$  are integrated before implementing the ridgelet transform. Finally, the ridgelet transform is performed after the renormalization step and it is described by equation (3).

$$\alpha_\mu = \langle h_Q, p\lambda \rangle \quad (3)$$

The de-noising results after applying the Curvelet transform are represented in Fig. 4.

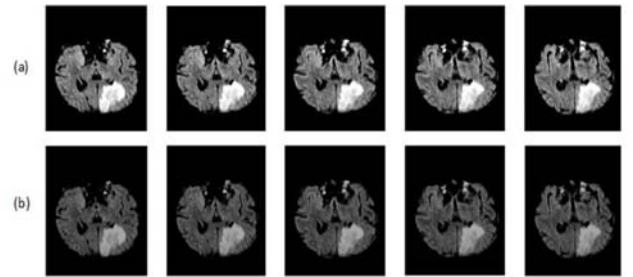


Fig. 4. Image de-noising by implementing Curvelet transform using MRI images of the brain from BRATS 2013 dataset. The upper row(a) represents original images while below row(b) explains enhanced images after Curvelet transform.

### 3.2. ACO and thresholding based tumor extraction

In the medical field, image segmentation is an essential and vital step due to its significance in the process of infection detection (Mehshan Ahmed Khan et al., 2020). The challenges of tumors such as irregular shape and change of texture are major limitations of this domain (Khan et al., 2020). These limitations affect the overall accuracy and complexity of the segmentation process. There are many methods used to overcome these limitations, such as expectation maximization (EM), Otsu thresholding, Watershed, and few more. In this research, a hybrid approach named as ACO and thresholding method for tumor segmentation is implemented. ACO (X. Wang et al., 2019) is employed for edge detection, and it is used with thresholding for the extraction of tumor region from a brain image. The input image is regarded as a graph which basically is two dimensional, and its nodes are pixels of the image. Ants travel from one pixel to another one on the graph for the sake of making a pheromone matrix whose every single entry is responsible for representing the edge information around every solo pixel site in an image. The relocation of ants is organized with the help of heuristic information. These ants alter their site in the image in accordance with the rules of transition and after that leave a pheromone particular quantity on those nodes that were visited by them. As much as the ants follow a track, the same amount or size of pheromone is observed. This eventually makes this trail more attractive for many other ants. Finally, the outcomes of the detection of edges can be acquired by doing an analysis of pheromone dispersal in the image. These technique implementation details are given as under:

#### Starting Ant Distribution-

Mostly, the quantity of ants is calculated mathematically by using equation (4).

$$N = \sqrt{A \times B} \quad (4)$$

Where, A = length of an input image, B = width of an input image and N is for the random placement of ants with an arrangement that at maximum only one ant can be on each pixel.

#### Decision-based on Probability-

An ant n travels with a probability  $p_{ij}$  from pixel (i, j) to pixel (k, l). The value of probability is calculated by equation (5).

$$p_{ij} = \frac{(\sigma_{ij})^\alpha (\mu_{ij})^\beta w_{ij}(\Delta)}{\sum_{j \in Q} (\sigma_{ij})^\alpha (\mu_{ij})^\beta w_{ij}(\Delta)}, \text{ when } i, j \in \Omega \quad (5)$$

Where, all the values of pixel locations which are 8-neighbourhood of the recent pixel (i, j) are shown by i, j  $\in \Omega$ .  $\sigma_{ij}$  symbolizes the amount of pheromone.  $\mu_{ij}$  denotes the visibility whose value is described by using the function given in equation (6).

$$\mu_{ij} = G_{ij} \quad (6)$$

In the equation of probability, the amount of variations in direction at each stage is calculated by  $\Delta$  plus it can use discrete or distinct value. This is given in equation (7).

$$\Delta = 0, \frac{\pi}{4}, \frac{\pi}{2}, \frac{3\pi}{4}, \pi. \quad (7)$$

Where,  $w(\Delta)$  symbolizes weighting function plus this function makes sure that the probability of very sudden plus sharp turns is less in comparison to the turns with smaller angles, hence every ant of colony retains a probabilistic bias in onward direction.

#### Rules of Transition-

The variable n represents an ant placed at pixel location (i, j) will travel to pixel location (k, l) with respect to equation (8)

$$s = \left\{ \arg \left\{ \max_{j \in \Omega} \left[ (\sigma_{ij})^\alpha (\mu_{ij})^\beta w_{ij}(\Delta) \right] \right\} \right\}, \text{ when } q \leq q_0 \quad (8)$$

If  $q > q_0$ , ants have the ability to choose the next pixel for visiting, as demonstrated by the probability distribution shown in part II.

#### Updating Pheromone-

The matrix of pheromone is required to be changed two times while the ACO process is still going on. First of all, once an ant gets transferred from the recent pixel (i, j) to the afterward pixel (k, l), the pheromone trajectory of its path is altered as given under in equation (9 and 10).

$$\sigma_{ij} = (1 - \gamma) \cdot \sigma_{ij} + \gamma \cdot \Delta \sigma_{ij} \quad (9)$$

$$\Delta \sigma_{ij} = \mu_{ij} \quad (10)$$

Where,  $\gamma (0 < \gamma < 1)$  shows the ratio of evaporation of pheromone.

The next change signifies global change on all the routes despite or not a route has been traversed. The pheromone gets the new value after each round, and the matrix of pheromone is updated accordingly as follows by equation (11).

$$\sigma_{ij} = (1 - \theta) \cdot \sigma_{ij} + \theta \cdot \sigma_0 \quad (11)$$

Where,  $\theta (0 < \theta < 1)$  denotes the ratio of pheromone evaporation and  $\sigma_0$  illustrates the pheromone starting value.

#### The procedure of final decision-

A pre-determined number of rounds are used to set the end of the algorithm; each of such cycles is comprised of fixed stages. At last, a binary decision is taken at every pixel site in order to decide if it was present on the outside border or not. This is done by implementing a threshold value T on the concluding resultant pheromone matrix.

Finally, irrelevant regions are removed with the help of thresholding, and its results are presented in Figures 5 and 6.

### 3.3. Feature Extraction

Feature extraction is a vital stage in ML to classify objects into their relevant category (Acharya et al., 2019; Khan et al., 2018; Khan et al., 2017; Manic et al., 2019; Raza et al., 2018; M. Sharif et al., 2017). Several categories of features are extracted in the literature, plus each feature has its own properties (Khan et al., 2018; Rashid et al., 2018; M. Sharif et al., 2018). In this paper, the exact location of the tumor in

brain MRI scans is determined after the extraction of shape as well as texture features.

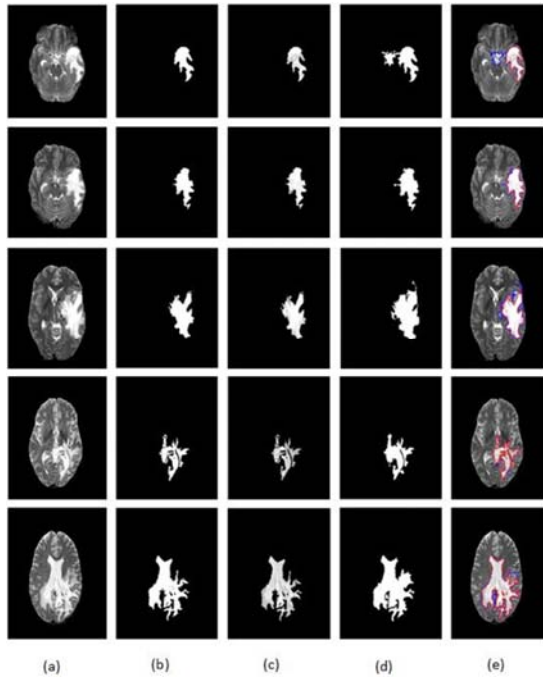


Fig. 5. Brain tumor segmentation results based on the hybrid technique of ACO+Thresholding using a private dataset. (a)Original image (b)Segmented image using ACO+Thresholding (c)Mapped image (d)Ground truth image (e)Mapping of the segmented image with ground truth image.

The performance accuracy of any method is dependent on the extraction process of the most robust and active set of features. LBP and SFTA features exist in the set of local features and extracted to get information about texture, whereas HOG descriptors are laid in the set of global features because of shape information. Furthermore, the explanation of all the extracted features is presented below.

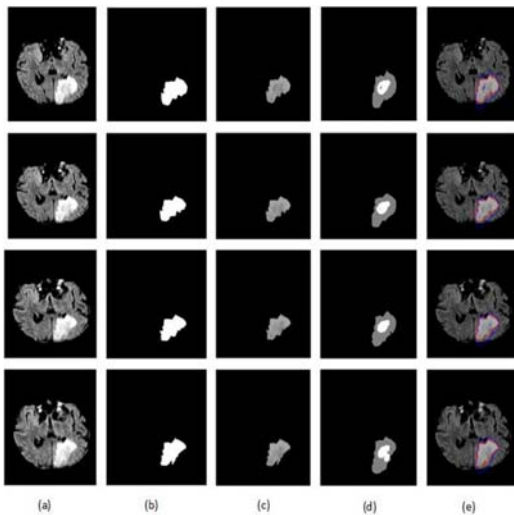


Fig. 6. Results of brain tumor segmentation using a hybrid system of ACO+Thresholding using the BRATS 2013 dataset. (a) Actual image (b) Image with segmentation using ACO+Thresholding (c) Plotted image (d) image of Ground truth (e)Plotting of segmented image with ground truth image

### Local Binary Patterns-

The texture patterns lie in the category of Local binary pattern(LBP) features that utilized in many ML applications because of low computational time, simplicity, and robustness (Rajesh and Malar, 2017). Mathematically, LBP features are computed as follows in equation (12).

$$LBP_{T,r} = \sum_{k=0}^{T-1} S(h_k - h_c)2^k, \quad (12)$$

When,  $S(x) = \{1, \text{ if } x \geq 0 \mid 0, \text{ if } x < 0\}$  (Yang et al., 2003). The variable  $T$  symbolizes, the number of pixels represent in the matrix, symbolizes the radius of the corresponding matrix,  $h_k$  is current pixel value and  $h_c$  is the central pixel value. This formulation provides a binary bit string that is further converted to a decimal string and then finally converted into a histogram. The resultant feature vector is obtained after converted into histograms of dimension  $N \times 59$ .

### Histogram of Oriented Gradient-

In the second phase, the extraction of features named as Histogram of oriented gradient (HOG)is performed on segmented tumor images. As (Wang et al., 2018) identification of an object with the help of its shape is accomplished using HOG features; therefore, the detection accuracy of the shape and appearance of an object depends upon dispersion of local intensity gradient and edge detection. There are four steps involved in HOG feature extraction, which include gradient calculation, separation of blocks and cells, normalization of blocks, and vector calculation. In the gradient calculation step, horizontal and vertical gradients are computed by using the mask  $[-1 \ 0 \ 1]^T$  and  $[-1 \ 0 \ 1]$  respectively. Mathematically, the mask is defined as follows by equations (13) and (14).

$$K_x(x, y) = L(x + 1, y) - L(x - 1, y) \quad (13)$$

$$K_y(x, y) = L(x, y + 1) - L(x, y - 1) \quad (14)$$

When,  $L(x, y)$  is the representation of pixel values,  $K_x(x, y)$  denotes the horizontal axis direction and  $K_y(x, y)$  is vertical direction, respectively. Then in the second step, the orientation and magnitude are computed by following mathematical formulation given in equations (15) and (16).

$$K(x, y) = \sqrt{K_x(x, y)^2 + K_y(x, y)^2} \quad (15)$$

$$b(x, y) = \tan^{-1} \left( \frac{K_y(x, y)}{K_x(x, y)} \right) \quad (16)$$

Where,  $K(x, y)$  describes the magnitude and  $b(x, y)$  represents the gradient direction. Afterward, an image given as input is distributed into sections, and each section is converted into cells of size  $8 \times 8$ . Each  $8 \times 8$  cell contains 192 values. Moreover, a histogram with 9 bin values is used for the representation of these values and later on these value stores into an array. The next step is about normalization block cell of size  $16 \times 16$  using the mathematical formulation as follows in equations (17) to (19).

$$V = [a_1, a_2, a_3, \dots, a_q] \quad (17)$$

$$VL = \sqrt{a_1^2 + a_2^2 + a_3^2 + \dots + a_q^2} \quad (18)$$



$$VN = \left[ \frac{a_1}{VL}, \frac{a_2}{VL}, \frac{a_3}{VL}, \dots, \dots, \frac{a_q}{VL} \right] \quad (19)$$

Where,  $V$  denotes the extracted vector,  $VL$  represents the length of the vector, which is equal to the norm and  $VN$  shows the normalized vector, respectively. Finally, a resultant vector of dimension  $N \times 3780$  is obtained.

#### Fractal Texture Analysis based on Segmentation (SFTA)-

The complexity and features based on texture in an image are demonstrated by SFTA (Costa et al., 2012; Zhelezniakov et al., 2015) using fractal dimension analysis. SFTA is very useful for the classification of texture. The computation process of SFTA features includes two steps, firstly a bunch of binary images is attained through the division of segmented image. Secondly, the computation of the fractal dimension is performed on sections of the binary image. The posterior probabilities, as given in equation (20), are calculated after giving 'a' to SFTA feature vector for each class  $C_n$  showing an earlier identified individual in a database.

$$p(C_n|a) = \frac{p(C_n)p(a|C_n)}{p(a)} \quad (20)$$

Where, class prior  $\text{top}(C_n)$  are computed by assuming classes as equi-probable. The ranking of classes depends upon posterior probabilities. Finally, a group of similar matches can be presented for decision making.

#### 3.4. Feature Reduction and Fusion

Feature reduction is an important step in the pattern recognition domain to reduce the number of predictors for fast execution of a system (Arshad et al., 2020). In the reduction techniques, mostly, the features are removed based on the heuristic approach (Mehmood et al., 2020). Many reduction techniques are presented in the medical imaging to improve the accuracy of a system and minimize the execution time (A Liaqat et al., 2020; Majid et al., 2020; Zahoor et al., 2020). In this step, a new technique named PCA reduced skewness (PCArS) is proposed for feature reduction. The proposed PCArS approach consists of two core steps- PCA based principle score (PS) calculation and skewness calculated from PS to reduce irrelevant features from each feature set. The resultants FVs are fused with respect to the simple serial-based concatenation process after reducing irrelevant features. Mathematically, the reduction and fusion process is defined as follows.

Let  $F_1$ ,  $F_2$  and  $F_3$  are three extracted feature vectors LBP, HOG, and SFTA, whereas the dimension of each vector is  $N \times 59$ ,  $N \times 3780$ , and  $N \times 21$  correspondingly. Let  $F_{s1}$ ,  $F_{s2}$  and  $F_{s3}$  denote the principle score values (PSV) of each FV which is mathematically formulated by equation (21).

$$\widehat{F_k(i)} = \bar{F}_i + z_{ki}M_{ki} \quad (21)$$

Where,  $\widehat{F_k(i)}$  denote the prediction of  $i$ th observation,  $i$  and  $j$  are rows and columns pixels, and  $M$  is an  $p \times p$  principle matrix. The variable  $\bar{F}_i$  is centroid or mean point of extracted vector. The PSV is computed for all three vectors  $F_1$ ,  $F_2$ , and  $F_3$ . After that, by utilizing PSV  $\widehat{F_k(i)}$ , we compute the skewness vector by using  $i$ th pixels as:

$$S(i)^h = \frac{\sum_{i=1}^N (F_i - \bar{F})^3 |N|}{(\sigma)^3} \quad (22)$$

Where,  $\bar{F}$  denotes the mean value,  $\sigma$  is a standard deviation and  $N$  are the total number of data points. The variable  $h \in (1,2,3)$  of LBP, HOG, and SFTA skewness vector. After that, only positive skewness values are considered for reduced FVs and serial-based fusion is performed (Yang et al., 2003). Finally, the top70% features are filtered from the fused vector and then given to multi-SVM of kernel function (RBF) where the number of splits is automatic.

## 4. RESULTS

In this part, the experimental results of the proposed segmentation and classification approach are described in both qualitative and quantitative forms. The new proposed system results are tested using two datasets- Private collected images and BRATS 2013.

The privately collected dataset consists a total of 80 images, including 40 healthy as well as 40 unhealthy MRI scans. These images are collected from Nishtar Hospital, Multan. They also provided their ground truths for segmentation analysis, as shown in Figure 5(d). The dimension of these images is  $512 \times 728$ . These images are only used for research purposes.

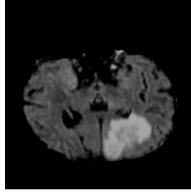

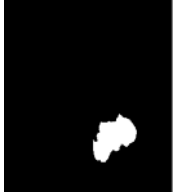
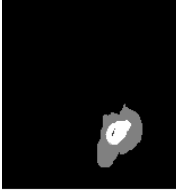
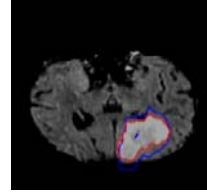
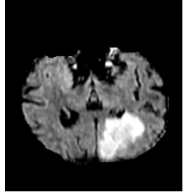


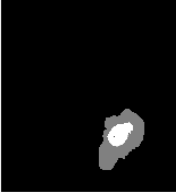
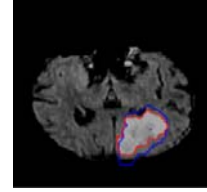
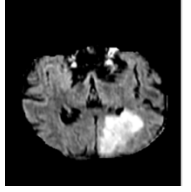

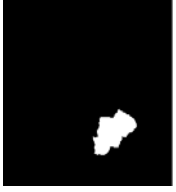

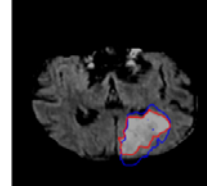
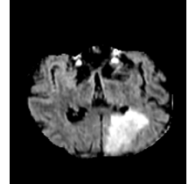

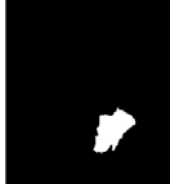

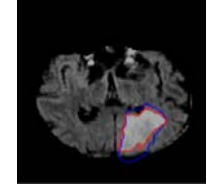
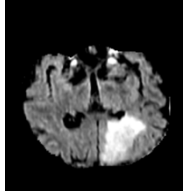


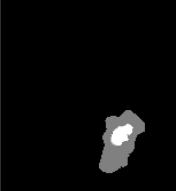
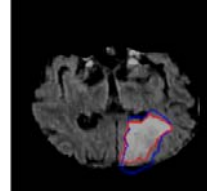
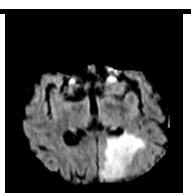
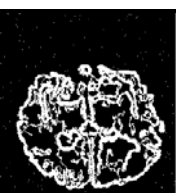
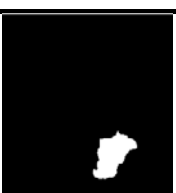
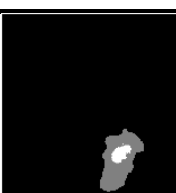
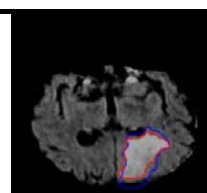
While on the other hand, BRATS 2013 dataset includes a total of 30 subjects (20 HG and 10 LG MRI scans). These scans include malignant, benign, and healthy images. Two different types of results are computed for the analysis of the proposed framework- segmentation results on selective Private and BRATS 2013 dataset and classification. The proposed classification performance is measured and compared with recently implemented classification algorithms such as ensemble trees and decision trees. The analysis of these classifiers is done through well-known performance metrics, including sensitivity, precision, accuracy, and FNR.

#### 4.1. Segmentation Results

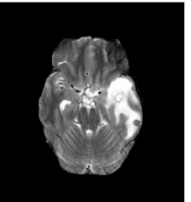


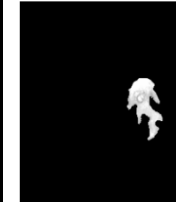
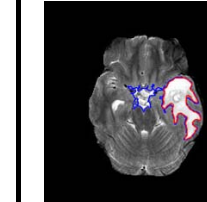
The accuracy of segmentation results is analyzed in this section on both Privately collected scans and a few BRATS 2013 dataset, respectively. The dice (D) parameter is computed for the validation of segmentation performance. The results are shown in Tables 1 and 2 for given two datasets.

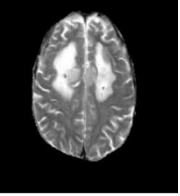
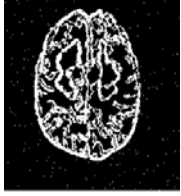


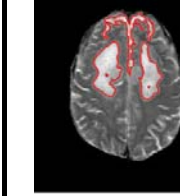
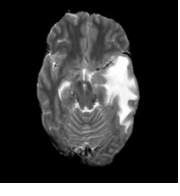



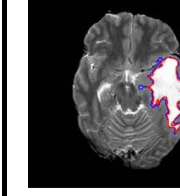
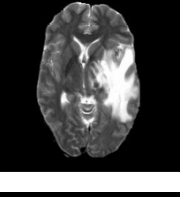



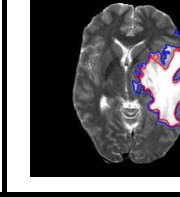
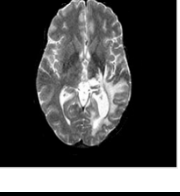
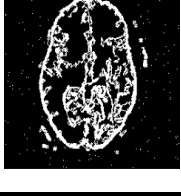


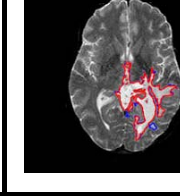

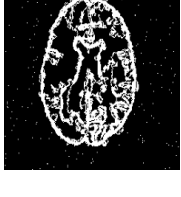


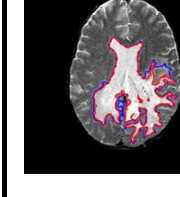
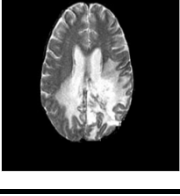
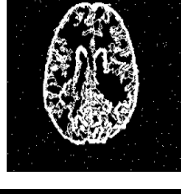


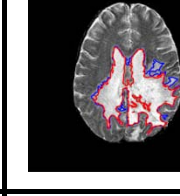
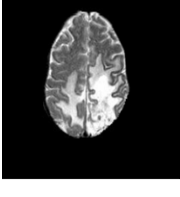
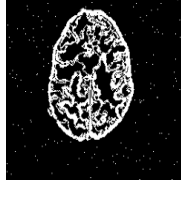


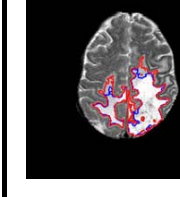
Some sample results alongside images of ground truth are presented in Table 1 to compute the average dice value of 90.81% which is significantly good. 100% accuracy is not possible in this case due to several factors such as change of tumor place, size, and orientation. In Table 2, segmentation results of the BRATS 2013 dataset are presented and achieved average segmentation dice is 95.29%, and FNR is 4.3%. The results are obtained through provided ground truth images. In Tables 1 and 2, each row consists of the following sequence- original scan, edge extraction, proposed segmented tumor, corresponding ground truth image, boundary extraction, and dice value. The average segmentation results demonstrate that the ACO along thresholding approach outperforms on both given datasets for the dice value.

**Table 1. Segmentation results of ACO along with thresholding on BRATS 2013 dataset.**

Actual Image	Edges Extraction	Segmented Image	Ground truth	Boundary image	Dice value
					0.9034
					0.9006
					0.8896
					0.8994
					0.9052
					0.9109

**Table 2. Segmentation results of ACO along with thresholding on Privately collected MRI scans.**

Actual Image	Edges Detection	Segmented Image	Ground truth	Boundary Extraction	Dice Value
					0.9191

					0.9422
					0.9237
					0.9484
					0.9208
					0.9167
					0.9977
					0.9748

#### 4.2. Classification Results

In this part, the results of the proposed classification approach are tested by using two datasets- BRATS 2013 as well as the Privately collected dataset. The accuracy of classification is measured through five performance metrics,

as discussed above. A 60:40 approach is selected, which explains that the training is performed on 60% of MRI scans from both datasets, and testing is performed on the remaining 40% scans. All results are computed with the help of K-fold cross-validation when K=10.



There are three steps involves for computation of classification results using the BRATS 2013 dataset- Fusion of reduced features after the PCArS approach, presented in Table 3. The highest gained accuracy of this step is 90.3%, which is verified in Table 4. The other best-achieved performance measures, which are known as sensitivity, precision, AUC, and FNR are 84.30%, 88.67%, 0.940, and 9.7%, respectively.

In step two, the computation results of classification based on the top 70% features plus gained the highest accuracy of 92% based on MSVM, shown in Table 5. The other calculated parameters as sensitivity, precision, AUC, and FNR are 91.33%, 91.67%, 0.903, and 8%, respectively. These results are also verified in Table 6.

The top 50% features are selected to perform classification in

the third step. The achieved maximum accuracy is 94.7% and the outcomes are demonstrated in Table 7 plus verified by Table 8. The overall results of classification by using the BRATS 2013 dataset demonstrates that the selection of 50% priority features gives better accuracy as compared to 70% top priority selected features and fusion of reduced feature vectors. Moreover, it is also clearly shown that MSVM outperforms as compared to ensemble and decision trees classification techniques.

In addition, the classification results of Privately collected MRI scans are shown in Table 9. The highest gained accuracy of MSVM on 50% reduced features is 94.6%, which is verified by Table 10. The other SVM Kernel functions also give good accuracy of 94.4%, which shows the consistency of overall results on the Private dataset.

**Table 3. Results of PCArS reduced features fusion by using BRATS 2013.**

Met	Performance Measures				
	Sen(%)	Pre(%)	AUC	Acc (%)	FNR(%)
Linear SVM	68.00	91.00	0.940	86.2	13.8
Quadratic SVM	80.00	84.00	0.936	89.4	10.6
Cubic SVM	75.67	82.00	0.917	88.4	11.6
Fine KNN	80.00	82.67	0.860	89.4	10.6
Cubic KNN	35.00	85.30	0.760	62.3	37.7
Cosine KNN	76.33	88.30	0.976	88.3	11.7
Fine Tree	69.33	71.00	0.830	77.4	22.6
Boosted Trees	70.67	79.00	0.927	80.7	19.3
Bagged Trees	49.00	58.33	0.810	70.9	29.1
<b>MSVM</b>	<b>89.67</b>	<b>88.67</b>	<b>0.940</b>	<b>90.3</b>	<b>9.7</b>

**Table 4. Confusion matrix of PCArS reduced features fusion by using BRATS 2013.**

Category	Category		
	Benign	Melanoma	Healthy
Benign	<b>92%</b>	4%	4%
Melanoma	9%	<b>84%</b>	3%
Healthy	6%	1%	<b>93%</b>

**Table 5. Proposed classification results on 70% priority features selection by using BRATS 2013.**

Method	Performance Measures				
	Sensitivity (%)	Precision (%)	AUC	Accuracy (%)	FNR (%)
Linear SVM	77.00	81.00	0.950	84.4	15.6
Q SVM	82.00	83.00	0.963	88.4	11.6
Cubic SVM	83.33	84.00	0.963	89.8	10.2
Fine KNN	85.13	86.67	0.903	92.0	8.0

Cubic KNN	73.00	84.00	0.953	84.1	15.9
Cosine KNN	81.67	89.00	0.983	89.1	10.9
Fine Tree	67.00	69.67	0.817	76.8	23.2
BT	67.33	73.33	0.900	77.1	22.9
Bagged Trees	80.00	82.00	0.927	86.8	13.2
<b>MSVM</b>	<b>91.33</b>	<b>91.67</b>	<b>0.903</b>	<b>92.0</b>	<b>8.0</b>

Table 6. Confusion matrix of 70% priority features selection by using BRATS 2013.

Category	Category		
	Benign	Melanoma	Healthy
Benign	<b>94%</b>	4%	2%
Melanoma	30%	<b>86%</b>	2%
Healthy	5%	1%	<b>94%</b>

Table 7. Proposed classification results on 50% top priority selected features by using BRATS 2013.

Method	Performance Measures				
	Sensitivity (%)	Precision (%)	AUC	Accuracy (%)	FNR (%)
Linear SVM	93.33	93.67	0.993	93.6	6.4
QSVM	92.67	93.00	0.983	92.8	7.2
Cubic SVM	92.33	92.67	0.983	92.4	7.6
Fine KNN	94.00	94.37	0.960	93.7	6.3
Cubic KNN	87.00	88.00	0.963	87.1	12.9
Cosine KNN	86.33	89.67	0.970	86.4	13.6
Fine Tree	82.00	82.00	0.890	82.2	17.8
Bagged Trees	91.33	91.67	0.977	91.3	8.7
SDA	94.33	94.33	0.993	94.3	5.7
<b>MSVM</b>	<b>94.33</b>	<b>94.67</b>	<b>0.957</b>	<b>94.7</b>	<b>5.3</b>

Table 8. Confusion matrix of top 50% selected features.

Category	Category		
	Benign	Melanoma	Healthy
Benign	94%	6%	
Melanoma	5%	94%	1%
Healthy	3%	1%	95%

Table 9. Proposed classification results on Private collected MRI scans.

Classifier	Performance Measures				
	Sensitivity (%)	Precision (%)	AUC	Accuracy (%)	FNR (%)
Linear SVM	94.5	95.0	0.89	94.4	5.6
QSVM	89.0	89.0	0.89	88.9	11.1

Cubic SVM	89.0	89.0	0.83	88.9	11.1
CGSVM	94.5	95.0	0.89	94.4	5.6
Cubic KNN	94.3	95.0	0.93	94.4	5.6
Cosine KNN	94.3	95.0	0.94	94.4	5.6
MKNN	94.3	95.0	0.94	94.4	5.6
Bagged Trees	89.0	89.0	0.94	88.9	11.1
EBT	89.0	91.0	1.00	88.9	11.1
<b>M-SVM</b>	<b>94.5</b>	<b>95.2</b>	<b>0.98</b>	<b>94.6</b>	<b>5.4</b>

**Table 10. Confusion matrix of Privately collected dataset.**

Category	Category	
	Healthy	Unhealthy
Healthy	<b>90%</b>	11%
Unhealthy		<b>100%</b>

#### 4.3. Discussion and Comparison

The detailed discussion and comparison of the proposed method are described in this section. There are five primary stages involved in this research, as demonstrated in Figure 3. The first stage is used for enhancement of an image, curvelet based transformation is employed, and visual outputs are represented in Figure 4. As a second stage, ACO plus thresholding approach is proposed for tumor segmentation whose effects are shown in Figures 5 and 6. The third stage is for the extraction of multi properties features, which are reduced in the next stage, which comes on no.4 by the PCaRS approach. On the final stage, the top 50% priority features are picked and are transferred to MSVM for the sake of classification. In the results section, initially, the segmentation results are presented in Tables 1 and 2 for BRATS 2013 and Private collected datasets, respectively. The overall achieved dice is higher than 90%. Finally, the classification results are presented in Tables 3-10 for both datasets and maximum achieved accuracy of 94% and 94.6%, respectively. The accuracy of classification using the BRATS 2013 dataset is computed in three steps- the fusion of reducing feature vectors, selection of top 70% priority features, and 50% top priority features. The overall results are demonstrating clearly that the system proposed gives the best performance for selecting the top 50% features.

Further, Table 11 provides a comparison of the proposed method and already implemented techniques in terms of accuracy measure. Reza et al. presented a technique depends on texture features to classify the tumor, with accuracy of 86.70%, which was tested upon the BRATS 2013 dataset and this approach. While this research concludes that segmentation is improved with the help of the hybrid technique of ACO and thresholding. The proposed hybrid segmentation method is implemented using the BRATS 2013 dataset and Private dataset providing an accuracy of 91.09% and 99.77%, respectively. Moreover, best classification results are attained by using skewness controlled PCA for

features selection with an accuracy of 94.7% and 94.4% for BRATS 2013 and Private datasets correspondingly.

**Table 11. Comparison of the proposed method with existing methods by using BRATS 2013 dataset.**

Approach	Year	Dataset	Accuracy Rate
(Cordier et al., 2013)	2013	BRATS 2013	84.00%
(Reza et al., 2015)	2015	BRATS 2013	86.70%
(Abbasi & Tajeripour, 2017)	2017	BRATS 2013	93.00%
<b>Proposed</b>	<b>2019</b>	<b>BRATS 2013</b>	<b>94.70%</b>

## 5. CONCLUSION

A unified framework has been proposed to segment and classifies brain tumor that is comprised of five primary steps. Curvelet transform is applied for tumor visibility enhancement, which is later segmented through ACO along with the thresholding method. Mixtures of texture and shape features are extracted and reduced through the PCaRS approach and serially fused all of them. Later, results are computed on all fused features, top 70% priority features, and 50% features. The classification accuracy of the top 50% features is shown best as compared to others. From results, it is concluded that better segmentation of the tumor provides useful features, which later on give the best accuracy. Moreover, it is also clear that the reduction of 50% features provides better accuracy, whereas, on 70% features, the results are consistent for all datasets.

In future work, the efficiency and accuracy of this system can be improved with the help of implementing deep learning. Deep learning is prevalent among researchers these days, and it can help to make system automated with great accuracy and efficiency (Muhammad Attique Khan, Tallha Akram, et al., 2020; Muhammad Attique Khan, Kashif Javed, et al., 2020). The proposed unified framework has some limitations, such as the selection of only the top 70% and 50% features and over-segmentation, which will be overcome in the future.

## ACKNOWLEDGMENT

Faculty Grant, HITEC University Taxila, Pakistan

## REFERENCES

- Abbasi, S., & Tajeripour, F. (2017). Detection of brain tumor in 3D MRI images using local binary patterns and histogram orientation gradient. *Neurocomputing*, 219, 526-535.
- Acharya, U. R., Fernandes, S. L., WeiKoh, J. E., Ciaccio, E. J., Fabell, M. K. M., Tanik, U. J., Yeong, C. H. (2019). Automated Detection of Alzheimer's Disease Using Brain MRI Images—A Study with Various Feature Extraction Techniques. *Journal of Medical Systems*, 43(9), 302.
- Afza, F., Khan, M. A., Sharif, M., & Rehman, A. (2019). Microscopic skin laceration segmentation and classification: A framework of statistical normal distribution and optimal feature selection. *Microscopy research and technique*.
- Akram, T., Khan, M. A., Sharif, M., & Yasmin, M. (2018). Skin lesion segmentation and recognition using multichannel saliency estimation and M-SVM on selected serially fused features. *Journal of Ambient Intelligence and Humanized Computing*, 1-20.
- Anitha, R., & Siva Sundhara Raja, D. (2018). Development of computer-aided approach for brain tumor detection using random forest classifier. *International Journal of Imaging Systems and Technology*, 28(1), 48-53.
- Ariyo, O., Zhi-guang, Q., & Tian, L. (2017). Brain MR Segmentation using a Fusion of K-Means and Spatial Fuzzy C-Means. *DEStech Transactions on Computer Science and Engineering(csae)*.
- Arshad, H., Khan, M. A., Sharif, M. I., Yasmin, M., Tavares, J. M. R., Zhang, Y. D., & Satapathy, S. C. (2020). A multilevel paradigm for deep convolutional neural network features selection with an application to human gait recognition. *Expert Systems*, e12541.
- Bahadure, N. B., Ray, A. K., & Thethi, H. P. (2018). Comparative Approach of MRI-Based Brain Tumor Segmentation and Classification Using Genetic Algorithm. *Journal of digital imaging*, 1-13.
- Buerki, R. A., Chheda, Z. S., & Okada, H. (2018). Immunotherapy of Primary Brain Tumors: Facts and Hopes. *Clinical Cancer Research*, 24(21), 5198-5205.
- Cordier, N., Menze, B., Delingette, H., & Ayache, N. (2013). *Patch-based segmentation of brain tissues*. Paper presented at the MICCAI challenge on multimodal brain tumor segmentation.
- Costa, A. F., Humpire-Mamani, G., & Traina, A. J. M. (2012). *An efficient algorithm for fractal analysis of textures*. Paper presented at the Graphics, Patterns and Images (SIBGRAPI), 2012 25th SIBGRAPI Conference on.
- Damodharan, S., & Raghavan, D. (2015). Combining Tissue Segmentation and Neural Network for Brain Tumor Detection. *International Arab Journal of Information Technology (IAJIT)*, 12(1).
- Drozdal, M., Chartrand, G., Vorontsov, E., Shakeri, M., Di Jorio, L., Tang, A., . . . Kadoury, S. (2018). Learning normalized inputs for iterative estimation in medical image segmentation. *Medical image analysis*, 44, 1-13.
- Fernandes, S. L., Tanik, U. J., Rajinikanth, V., & Karthik, K. A. (2019). A reliable framework for accurate brain image examination and treatment planning based on early diagnosis support for clinicians. *Neural Computing and Applications*, 1-12.
- Kalavathi, P., & Prasath, V. S. (2016). Methods on skull stripping of MRI head scan images—A review. *Journal of digital imaging*, 29(3), 365-379.
- Khan, M. A., Akram, T., Sharif, M., Awais, M., Javed, K., Ali, H., & Saba, T. (2018). CCDF: Automatic system for segmentation and recognition of fruit crops diseases based on correlation coefficient and deep CNN features. *Computers and Electronics in Agriculture*, 155, 220-236.
- Khan, M. A., Akram, T., Sharif, M., Javed, K., Raza, M., & Saba, T. (2020). An automated system for cucumber leaf diseased spot detection and classification using improved saliency method and deep features selection. *Multimedia Tools and Applications*, 1-30.
- Khan, M. A., Akram, T., Sharif, M., Saba, T., Javed, K., Lali, I. U., . . . Rehman, A. (2019). Construction of saliency map and hybrid set of features for efficient segmentation and classification of skin lesion. *Microscopy research and technique*, 82(6), 741-763.
- Khan, M. A., Javed, K., Khan, S. A., Saba, T., Habib, U., Khan, J. A., & Abbasi, A. A. (2020). Human action recognition using fusion of multiview and deep features: an application to video surveillance. *Multimedia Tools and Applications*, 1-27.
- Khan, M. A., Khan, M. A., Ahmed, F., Mittal, M., Goyal, L. M., Hemanth, D. J., & Satapathy, S. C. (2020). Gastrointestinal diseases segmentation and classification based on duo-deep architectures. *Pattern Recognition Letters*, 131, 193-204.
- Khan, M. A., Sharif, M., Akram, T., Bukhari, S. A. C., & Nayak, R. S. (2020). Developed Newton-Raphson based deep features selection framework for skin lesion recognition. *Pattern Recognition Letters*, 129, 293-303.
- Khan, M. A., Sharif, M., Javed, M. Y., Akram, T., Yasmin, M., & Saba, T. (2017). License number plate recognition system using entropy-based features selection approach with SVM. *IET Image Processing*, 12(2), 200-209.
- Khan, M. A., Sharif, M. I., Raza, M., Anjum, A., Saba, T., & Shad, S. A. (2019). Skin lesion segmentation and classification: A unified framework of deep neural network features fusion and selection. *Expert Systems*, e12497.
- Liaqat, A., Khan, M., Sharif, M., Mittal, M., Saba, T., Manic, K., & Al Attar, F. (2020). Gastric Tract Infections Detection and Classification from Wireless Capsule Endoscopy using Computer Vision Techniques: A Review. *Current Medical Imaging*.
- Liaqat, A., Khan, M. A., Shah, J. H., Sharif, M., Yasmin, M., & Fernandes, S. L. (2018). Automated ulcer and bleeding classification from wce images using multiple features fusion and selection. *Journal of Mechanics in Medicine and Biology*, 1850038.
- Liu, J., Li, M., Wang, J., Wu, F., Liu, T., & Pan, Y. (2014). A survey of MRI-based brain tumor segmentation methods. *Tsinghua Science and Technology*, 19(6), 578-595.

- Majid, A., Khan, M. A., Yasmin, M., Rehman, A., Yousafzai, A., & Tariq, U. (2020). Classification of stomach infections: A paradigm of convolutional neural network along with classical features fusion and selection. *Microscopy research and technique*, 83(5), 562-576.
- Manic, K. S., Hasoon, F. N., Al Shibli, N., Satapathy, S. C., & Rajinikanth, V. (2019). *An Approach to Examine Brain Tumor Based on Kapur's Entropy and Chan-Vese Algorithm*. Paper presented at the Third International Congress on Information and Communication Technology.
- Mehmood, A., Khan, M. A., Sharif, M., Khan, S. A., Shaheen, M., Saba, T., . . . Ashraf, I. (2020). Prosperous Human Gait Recognition: an end-to-end system based on pre-trained CNN features selection. *Multimedia Tools and Applications*.
- Mohsen, H., El-Dahshan, E.-S. A., El-Horbaty, E.-S. M., & Salem, A.-B. M. (2018). Classification using deep learning neural networks for brain tumors. *Future Computing and Informatics Journal*, 3(1), 68-71.
- Nasir, M., Attique Khan, M., Sharif, M., Lali, I. U., Saba, T., & Iqbal, T. (2018). An improved strategy for skin lesion detection and classification using uniform segmentation and feature selection based approach. *Microscopy research and technique*.
- Pereira, S., Pinto, A., Alves, V., & Silva, C. A. (2016). Brain tumor segmentation using convolutional neural networks in MRI images. *IEEE transactions on medical imaging*, 35(5), 1240-1251.
- Rajesh, T., & Malar, R. (2017). Robust Classification of Brain Tumor in MRI Images using Salient Structure Descriptor and RBF Kernel-SVM. *Asian Journal of Research in Social Sciences and Humanities*, 7(2), 58-71.
- Rashid, M., Khan, M. A., Sharif, M., Raza, M., Sarfraz, M. M., & Afza, F. (2018). Object detection and classification: a joint selection and fusion strategy of deep convolutional neural network and SIFT point features. *Multimedia Tools and Applications*, 1-27.
- Raza, M., Sharif, M., Yasmin, M., Khan, M. A., Saba, T., & Fernandes, S. L. (2018). Appearance based pedestrians' gender recognition by employing stacked auto encoders in deep learning. *Future Generation Computer Systems*, 88, 28-39.
- Rehman, A., Khan, M. A., Mehmood, Z., Saba, T., Sardaraz, M., & Rashid, M. (2020). Microscopic melanoma detection and classification: A framework of pixel-based fusion and multilevel features reduction. *Microscopy research and technique*.
- Reza, S. M., Mays, R., & Iftikharuddin, K. M. (2015). *Multi-fractal detrended texture feature for brain tumor classification*. Paper presented at the Medical Imaging 2015: Computer-Aided Diagnosis.
- Roberts, T., Hyare, H., Hipwell, B., Ianus, A., Breen-norris, J., Panagiotaki, E., . . . Brandner, S. (2018). Quantification of tumour microstructure in low and high-grade brain tumours using VERDICT MRI: an initial feasibility study. *Neuro-oncology*, 20(suppl\_1), i16-i16.
- Routray, S., Ray, A. K., & Mishra, C. (2018). Image denoising by preserving geometric components based on weighted bilateral filter and curvelet transform. *Optik*, 159, 333-343.
- Safdar, A., Khan, M. A., Shah, J. H., Sharif, M., Saba, T., Rehman, A., . . . Khan, J. A. (2019). Intelligent microscopic approach for identification and recognition of citrus deformities. *Microscopy research and technique*.
- Sharif, M., Khan, M. A., Akram, T., Javed, M. Y., Saba, T., & Rehman, A. (2017). A framework of human detection and action recognition based on uniform segmentation and combination of Euclidean distance and joint entropy-based features selection. *EURASIP Journal on Image and Video Processing*, 2017(1), 89.
- Sharif, M., Khan, M. A., Iqbal, Z., Azam, M. F., Lali, M. I. U., & Javed, M. Y. (2018). Detection and classification of citrus diseases in agriculture based on optimized weighted segmentation and feature selection. *Computers and Electronics in Agriculture*, 150, 220-234.
- Sharif, M. I., Li, J. P., Khan, M. A., & Saleem, M. A. (2020). Active deep neural network features selection for segmentation and recognition of brain tumors using MRI images. *Pattern Recognition Letters*, 129, 181-189.
- Sharma, M., Purohit, G., & Mukherjee, S. (2018). Information retrieves from brain MRI images for tumor detection using hybrid technique K-means and artificial neural network (KMANN) *Networking communication and data knowledge engineering* (pp. 145-157): Springer.
- Starck, J.-L., Candès, E. J., & Donoho, D. L. (2002). The curvelet transform for image denoising. *IEEE Transactions on image processing*, 11(6), 670-684.
- Wang, X., Ouyang, J., Zhu, Y., Yu, H., & Li, H. (2019). A Novel Medical Image Edge Detection Method Based on Reinforcement Learning and Ant Colony Optimization. *Journal of Medical Imaging and Health Informatics*, 9(1), 175-182.
- Wang, Y., Zhu, X., & Wu, B. (2018). Automatic detection of individual oil palm trees from UAV images using HOG features and an SVM classifier. *International Journal of Remote Sensing*, 1-15.
- Yang, J., Yang, J.-y., Zhang, D., & Lu, J.-f. (2003). Feature fusion: parallel strategy vs. serial strategy. *Pattern recognition*, 36(6), 1369-1381.
- Zahoor, S., Lali, I. U., Khan, M., Javed, K., & Mehmood, W. (2020). Breast Cancer Detection and Classification using Traditional Computer Vision Techniques: A Comprehensive Review. *Current Medical Imaging*.
- Zhang, W., Li, R., Deng, H., Wang, L., Lin, W., Ji, S., & Shen, D. (2015). Deep convolutional neural networks for multi-modality isointense infant brain image segmentation. *NeuroImage*, 108, 214-224.
- Zhelezniakov, A., Eerola, T., Koivuniemi, M., Auttila, M., Levänen, R., Niemi, M., . . . Kälviäinen, H. (2015). *Segmentation of saimaa ringed seals for identification purposes*. Paper presented at the International Symposium on Visual Computing.